Climate Resilience and Sustainability
Open Access
Interdisciplinary Approaches Towards Solutions for Climate Change
RMetS
Royal Meteorological Society

ORIGINAL ARTICLE

Impact of merging of historical and future climate data sets on land carbon cycle projections for South America

Chris Huntingford[1] | **Stephen A. Sitch[2]** | **Michael O'Sullivan[3]**

[1] UK Centre for Ecology and Hydrology, Wallingford, UK

[2] College of Life and Environmental Sciences, University of Exeter, Exeter, UK

[3] College of Engineering, Mathematics and Physical Sciences, University of Exeter, Exeter, UK

Correspondence
Chris Huntingford, UK Centre for Ecology and Hydrology, Wallingford OX10 8BB, UK.
Email: chg@ceh.ac.uk

Abstract

Earth System Models (ESMs) project climate change, but they often contain biases in their estimates of contemporary climate that propagate into simulated futures. Land models translate climate projections into surface impacts, but these will be inaccurate if ESMs have substantial errors. Bias concerns are relevant for terrestrial physiological processes which often respond non-linearly (i.e. contain threshold responses) and are therefore sensitive to absolute environmental conditions as well as changes. We bias-correct the UK Met Office ESM, HadGEM2-ES, against the CRU–JRA observation-based gridded estimates of recent climate. We apply the derived bias corrections to future projections by HadGEM2-ES for the RCP8.5 scenario of future greenhouse gas concentrations. Focusing on South America, the bias correction includes adjusting for ESM estimates that, annually, are approximately 1 degree too cold, for comparison against 21st Century warming of around 4 degrees. Locally, these values can be much higher. The ESM is also too wet on average, by approximately 1 mm·day^{-1}, which is substantially larger than the mean predicted change. The corrected climate fields force the Joint UK Land Environment Simulator (JULES) dynamic global vegetation model to estimate land surface changes, with an emphasis on the carbon cycle. Results show land carbon sink reductions across South America, and in some locations, the net land–atmosphere CO_2 flux becomes a source to the atmosphere by the end of this century. Transitions to a CO_2 source is where increases in plant net primary productivity are offset by larger enhancements in soil respiration. Bias-corrected simulations estimate the rise in South American land carbon stocks between pre-industrial times and the end of the 2080s is ~12 GtC lower than that without climate bias removal, demonstrating the importance of merging historical observational meteorological forcing with ESM diagnostics. We present evidence for a substantial climate-induced role of greater soil decomposition in the fate of the Amazon carbon sink.

KEYWORDS
Amazon dieback, CO_2 fertilization, global warming, rainforest, soil respiration, South America climate change

1 | INTRODUCTION

Climate change is a defining issue of our time. To understand and derive robust mitigation strategies to climate change requires accurate estimates of near-surface climate and its change under differing greenhouse gas (GHG) emissions scenarios. The projections of Earth System Models (ESMs) guide most of climate research. In particular, ESM predictions of future change, and including alteration to near-surface meteorological conditions, underpin the science described in the regular Intergovernmental Panel on Climate Change reports (e.g. IPCC, 2013). ESMs strive to emulate the characteristics of the atmosphere, oceans, land surface and polar ice conditions, their interactions and response to rising GHGs. Numerical sub-models of climate system components are calibrated and tested against appropriate data sets from the recent past, and an ESM is their combination. ESMs require a period of numerical 'spin-up' to an equilibrium climatic state, representative of the pre-industrial period. The final part of the spin-ups is checked that there are no background drifts which, if present in subsequent transient calculations, will affect projections of change. The end of the spin-up generates the initial conditions for the transient calculations that determine climate responses as GHG levels change from their pre-industrial values. This numerical structure means that ESMs estimate the period between pre-industrial times and present, in addition to the decades ahead. Historical estimates allow comparison of ESM outputs against gridded data sets of past meteorological conditions based on weather station measurements or re-analysis products that entrain such meteorological data. Although checking spin-ups can help confirm no model drifts (i.e. time-evolving biases), overall model biases may remain which for even key quantities such as global mean temperature levels can be substantial (Palmer and Stevens, 2019). Under the assumption that these errors are likely to propagate into simulations of future periods, we can remove them to refine estimates of any climate change ahead. Such bias correction also ensures a smooth transition between the present-day end to historical observation-based data sets and model-based projections of future change. Hence, corrections allow the combined use of historical data, followed by more accurate ESM-based assessment of future climate, and with no jumps in time series for the present day. These combined estimates of evolving near-surface climate are available to drive terrestrial impacts models. As many ecosystem processes depend on the absolute value of near-surface climate conditions, bias-corrected drivers will likely enhance how well they are modelled.

Recently available is an advanced estimate of historical meteorological conditions, called the CRU–JRA data set (Harris, 2019a; Harris, 2019b). This data set is at six-hourly intervals, and is a merging of the monthly Climate Research Unit (CRU) gridded climatology (Harris et al., 2014) with the Japanese Re-Analysis product (JRA) (Kobayashi et al., 2015). We have selected CRU–JRA because of its application in the annual Global Carbon Budget assessments (Friedlingstein et al., 2020), and it offers an opportunity to be used to bias-correct an ESM. Such bias-corrected ESM output is then available to drive Dynamic Global Vegetation Model (DGVM) simulations into the near- (~year 2030) and long-term future (towards 2100). This modelling combination estimates changes in regional biogeochemistry and the provision of land ecosystem services. Such projections may also include how the global land carbon cycle will evolve, and thus is of importance to determining future global carbon stocktakes. Such stocktakes attract much interest for the tropics. Neotropical ecosystems are potentially highly vulnerable to climate change, with the possibility of eventual widespread forest loss in Amazonia caused by more drought-like conditions overtaking any CO_2-fertilization effects (Malhi et al., 2009; Huntingford et al., 2013). Ultimately, if climate-biophysical feedbacks become positive, by returning CO_2 to the atmosphere, they will amplify initial forest loss by adding further to ongoing climate change (Cox et al., 2000). It is still an open question as to whether and how close the Amazon forest is to a climate-induced 'die-back' tipping point, but as Malhi et al. (2009) demonstrate, bias-correcting forcing is important to inform accurately this debate.

Much recent research has focused on the direct physiological effects of global warming, with the suggestion that many ecosystems may be already operating above their high temperature optimum (Duffy et al., 2021). Additional to background warming trends, Amazon forests have also experienced especially high temperature levels during recent specific years. Such years include during the 2015/2016 El Niño, with the warmest September over the past decades occurring in year 2015, having temperatures about 1°C higher than even the last two drought years of 2005 and 2010 (Jardine et al., 2017). Unlike extratropical ecosystems which experience strong seasonality in temperature, tropical forests are adapted to a more stable temperature regime, and thus may have a sharp temperature optimum for key physiological processes. These ecosystems, which potentially have a restricted ability to acclimate to warming, may thus be especially sensitive to high temperatures (Booth et al., 2012). Furthermore, maximum temperature is the most important determinant of tropical biomass (Sullivan et al., 2020) and may contribute to potential declines in the Amazon carbon sink strength as mortality rates are increasing faster than productivity enhancements (Brienen et al., 2015; Hubau et al., 2020). Taken together, it is hypothesized that heat stress may be the most important driver of future neotropical forest change. It is

therefore imperative to calibrate vegetation models against data and drive them with bias-corrected climate fields for such sensitive ecosystems.

Less well documented is the role of soil respiration in the net land carbon sink for tropical regions. It is known that carbon stocks in tropical forest soils (10–15 kg C·m^{-2}) are comparable to those in biomass in lowland forests (∼15.4 kg C·m^{-2}) (Phillips et al., 2016; Jackson et al., 2017). A field soil warming experiment in Panama demonstrates an increase in heterotrophic respiration by over 50% with a 4°C warming (Nottingham et al., 2020). At that location, there is no evidence at the higher imposed temperatures of acclimation or a lowering of temperature sensitivity of enzyme activity. An extrapolation is made of this finding across the whole pan-tropical forests, leading to an estimate of potential soil C emissions of 65 PgC from a total soil C stock of ∼500 PgC over this century (Nottingham et al., 2020). Here, we can test this simple extrapolation by process-based modelling.

In this paper, we first generate a new merged historical and future climate forcing data set, and document the magnitude of biases removed relative to the expected future changes to climate. We then use this forcing as input to a process-based DGVM, to simulate the impact of future climate change on both water and carbon variables, given the intrinsic relation between these two cycles. Water changes can also be used to infer changes in the regional provision of a wider set of key ecosystem services, for example freshwater provision and downstream rainfall recycling. However, our main focus is to project the future change in the land carbon sink over South America and elaborate on the relative contribution of plant and soil processes to these changes.

2 | METHODS

2.1 | Monthly bias correction of HadGEM2-ES data

We start by considering six regional monthly near-surface meteorological fields of temperature, specific humidity, windspeed, precipitation, downward shortwave and downward longwave radiation. These quantities are selected as required, although at sub-daily timescales, by the Joint UK Land Environment Simulator (JULES) land model (Section 2.3). We first extract the monthly mean values of each of these fields, for the historical period, from the CRU–JRA gridded data, against which we bias-correct the HadGEM2-ES ESM (Jones et al., 2011). The CRU–JRA data set uses the JRA re-analysis product to provide sub-daily information, normalized against the CRU monthly climatology. This data set is on a 0.5° × 0.5° scale, and we use a version

aggregated to a spatial grid of 1.25° in latitude and 1.875° in longitude, which is identical to that of the HadGEM2-ES model. The monthly fields from CRU–JRA are saved for each location, and we also derive a set where we undertake spatial averaging over all neighbouring land points, in a rectangle of ±3° in latitudinal direction and ±2° in longitudinal direction. We design this spatial averaging to better capture the background climatic trends, by removing potential noise at single locations. For this spatially averaged data, we calculate linear trends for each month, location and the six key variables. These linear trends are for the 21 recent years of the CRU–JRA data, up to year 2018, fitted by standard regression. We then take the mean of this regression that accounts for spatial averaging, and the mean of last 21 years of actual data at the location, and add an offset to the regression such that the mean of the former equals that of the latter. This provides a linear estimate of the background trend, where the gradient value includes information by spatial averaging across adjacent points, but the actual magnitude of the values matches the specific details of the local point.

For the HadGEM2-ES data, we again calculate the spatial means across adjacent gridboxes, for each month and each variable. Temporally, we then calculate the 21-year centred running means, and throughout the time period that HadGEM2-ES simulates. Using running means rather than a regression accounts for nonlinear variation in background trends over the full range of the ESM projections. We use HadGEM2-ES diagnostics for that ESM as extracted from the Coupled Model Intercomparison Project v5 (CMIP5) database (Taylor et al., 2012). Our values correspond to the RCP8.5 concentration scenario that is sometimes called, in terms of related emissions, 'business-as-usual' (Meinshausen et al., 2011). Our bias correction of HadGEM2-ES is to then offset these running means (for each month, variable and location) such that their value for year centred on 2018 is equal to that of year 2018 from the fitted linear gradients to the CRU–JRA data. Our monthly mean climatological drivers, that we refer to as bias-corrected, are therefore those of CRU–JRA directly starting at year 1901, merging smoothly (in absolute values) at year 2018 into those of corrected HadGEM2-ES, for projection onwards towards 2100. The actual final year is 2089, due to using 21-year running means. We present in Figure 1 the algorithm graphically and for a sample gridbox containing the city of Manaus.

2.2 | Annual to six-hourly variation in climate

The second part of the normalization of HadGEM2-ES involves adjusting for the higher frequency variations. This
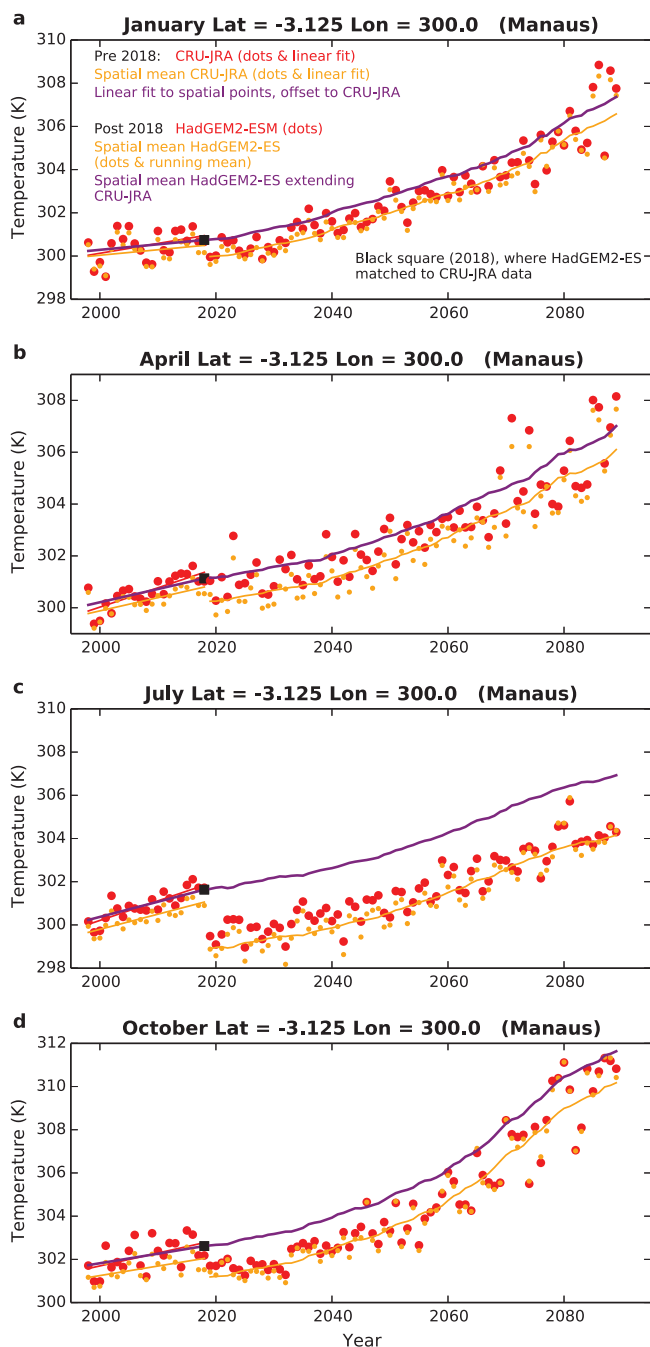
FIGURE 1 Bias-correction method. Monthly mean temperature (shown for January, April, July and October) for the gridbox containing the city of Manaus. Curves in the period to year 2018 are based on the data-led CRU–JRA climatology, whereas after that year, the diagram uses projections with the HadGEM2-ES ESM. Pre-2018, the red dots are for 21 years (1998–2018) at the individual gridbox, with a linear fit shown for information. Yellow dots are spatial means of the monthly values, including nearby points (±3° latitudinally, ±2° longitudinally), and shown with their linear fit (also yellow). The latter linear fit, so including the averaging of neighbouring points, we regard as a better estimate of trends by removing local fluctuations. This trend (yellow line) is then offset, so that its mean value equals that of the red dots for the single gridbox. We show this final linear fit in purple, and regard it as our estimate of background trends for the Manaus gridbox, pre-2018. For

allows the removal of errors in ESM projections of climate variability and higher-frequency weather fluctuations. The process also contributes further to a smooth transition between measurements from the contemporary period and model-based future projections. To achieve this, we calculate the anomalies between the 6-hourly CRU–JRA gridded data and the fitted linear regression for monthly values, as based on years 1998–2018 inclusive. We save these differences, and then add them to future bias-corrected running means from HadGEM2-ES, and for a repeating cycle of period 21 years. This procedure assumes that variability, from sub-daily up to decadal, is broadly invariant under climate change. However, this assumption may still aid more accurate future projections than using directly high-frequency variations from our ESM. Hence, what we now refer to our bias-corrected forcing data spans from 1901 to 2089. These forcing values are the direct measurement-based CRU–JRA data to year 2018, followed by our HadGEM2-ES normalized 21-year running means with the addition of CRU–JRA-based high-frequency variability.

2.3 | JULES land surface DGVM

JULES (Best et al., 2011; Clark et al., 2011) is the land component of the Hadley Centre climate model (Sellar et al., 2019). The model version we use is v5.4, setup as 'JULES-ES', and so has an identical framework to that used directly in an Earth System Model (Sellar et al., 2019). JULES-ES is also the configuration used in the recent Global Carbon Budget assessments (Friedlingstein et al., 2019, 2020; Table S1). JULES operates at an hourly time step, providing its own temporal dis-aggregation from our 6-hourly forcing data (Section 3.2). Also required is near-surface atmospheric pressure, although for these we simply use the historical means from CRU–JRA throughout. The model has a dynamic interactive vegetation part and includes vegetation competition, and so we henceforth

the period after 2018, red dots are HadGEM2-ES-based estimates for the individual gridbox, and yellow are averaged over neighbouring points (same spatial range as for CRU–JRA). The yellow curve is the 21-year running mean of spatially averaged HadGEM2-ES outputs, and for similar reasons to those of the data pre-2018, we regard this as representative of background trends. Finally, the yellow curve of running means for HadGEM2-ES is re-coloured as purple and offset to have an identical value in 2018 (black square) as the CRU–JRA-based purple trend for the same year. It is these calculated offsets, for each month, that are the basis of our bias correction fields. Hence, the purple curve from 2018 onwards is our estimate of future bias-corrected HadGEM2-ES projections, ready for adding high-frequency forcing to drive the JULES DGVM

HUNTINGFORD ET AL.

Climate Resilience and Sustainability
Interdisciplinary Approaches Towards Solutions for Climate Change | Open Access | RMetS | 5 of 17

refer to it as a DGVM. The competition part translates climate-driven changes in carbon fluxes, and in particular accumulated Net Primary Productivity (NPP), to altered fractional covers of Plant Functional Types (PFTs) and their carbon stores (Cox, 2001; Clark et al., 2011; Harper et al., 2018). Our version of JULES DGVM represents vegetation at each numerical gridbox with up to nine varying PFTs of broadleaf tropical and temperate evergreen trees, broadleaf deciduous, needleleaf evergreen and deciduous trees, C_3 (temperate) and C_4 (tropical) grasses, and evergreen and deciduous shrubs. Additional to these PFTs are fractions of C_3 crop and pasture, and C_4 crop and pasture, although with our focus on natural vegetation, these are fixed at year 1900 coverage. Hence, with land use held at near pre-industrial levels, we constrain our analysis to explore the impact of climate change on natural carbon cycling. Plant physiology in JULES is described by a coupled scheme of leaf photosynthesis and stomatal conductance, and temperature-dependent autotropic respiration. Our version of JULES includes a multi-layer canopy scheme for light interception, accounting for sunfleck penetration (Mercado et al., 2009), although we assume that the related prescription of the fraction of downward shortwave radiation that is diffuse radiation is invariant with a value of 0.4. This fractional value is the optimum to maximize Gross Primary Productivity (GPP) (e.g. figure S1 of Mercado et al., 2009 and figure 6 of Knohl and Baldocchi, 2008). We note, though, that multi-year gridded data sets of diffuse radiation are becoming available from either satellite (e.g. MODIS; Ryu et al., 2018) or other recently released re-analysis products (e.g. ERA5; Hersbach et al., 2020). JULES simulates surface CO_2 fluxes associated with photosynthesis and autotropic respiration using PFT-specific parameters aligned to observations (Harper et al., 2016, 2018). Based on tissue turnover rates, JULES simulates litterfall which enters the soil.

A soil carbon scheme determines the climate-modified rate of microbial soil respiration and the related flux of CO_2 back to the atmosphere. Specifically, heterotrophic respiration varies with soil temperature, following a Q_{10} formulation, and soil moisture. Soil moisture modulates respiration by a multiplicative scaling factor that is fixed and low for very dry soils, then increases linearly to unity for rising soil moisture. Then beyond when this value of unity is achieved, and so for very wet soils, the factor starts to decline again (Clark et al., 2011). We use a four-pool (layer) soil moisture model, based on the RothC model (Jenkinson, 1990; Jones et al., 2005; Clark et al., 2011). Respiration is calculated for a bulk soil carbon pool but using temperature and moisture values taken from the second soil layer.

Additional to the inputs to the JULES model of sub-daily meteorological driving data are prescribed changes in atmospheric CO_2 and ancillary information on soil texture. The rising CO_2 concentrations are consistent with the RCP8.5 scenario to which the plant physiology additionally responds to. A summary of all the component configurations of JULES is provided in Table S1.

3 | RESULTS

3.1 | Climate changes across South America

We present the effect of mean bias correction for temperature, for four representative months, and at a single location of the gridbox containing the city of Manaus (Figure 1). The main curve of interest is the purple one, which is a background trend for each month, fitted to the historical data until year 2018, followed by bias-corrected running mean future projections from the HadGEM2-ES ESM. For all 4 months shown, the ESM projects temperatures that are too cool, and this is especially for the month of July, that is during the dry season in parts of Amazonia (compare purple curves to yellow curves, post 2018). All the other curves and data points in Figure 1 illustrate the algorithm leading to the purple curve, as explained in the text above (Section 2.1) and the figure caption. The high temporal resolution data required to drive the JULES DGVM beyond year 2018 are built by adding variability to the purple curve for future times (not shown). We base this addition on past variations described by the CRU–JRA data, covering timescales from interannual variation down to 6 hourly (Section 2.2).

Across South America, we compare the magnitude of HadGEM2-ES biases in annual mean temperature and precipitation to their projected changes under RCP85 over the period between years 1999–2019 and years 2069–2089 (Figure 2). The first column of Figure 2 is the annual mean of the monthly offsets (i.e. bias corrections), presented as original HadGEM2-ES diagnostics minus CRU–JRA climatology. Our ESM is too cold across most of South America, matching the single gridbox assessment in Figure 1. The ESM is also slightly too dry in the central Amazon and too wet in eastern Brazil and over the Andes. The middle column of Figure 2 is the standard deviation of the monthly offsets at each location. HadGEM2-ES projects climate change to include a large increase in temperature, but relatively small changes in precipitation (third column). Spatially, one observes decreases in precipitation in Amazonia and increases in precipitation over the SE Brazil, associated with shifts in the South Atlantic Convergence Zone (SACZ). For some locations, biases in temperature are approaching the same order-of-magnitude as their projected changes as GHGs rise, whereas erroneous offsets in precipitation are substantially larger than their
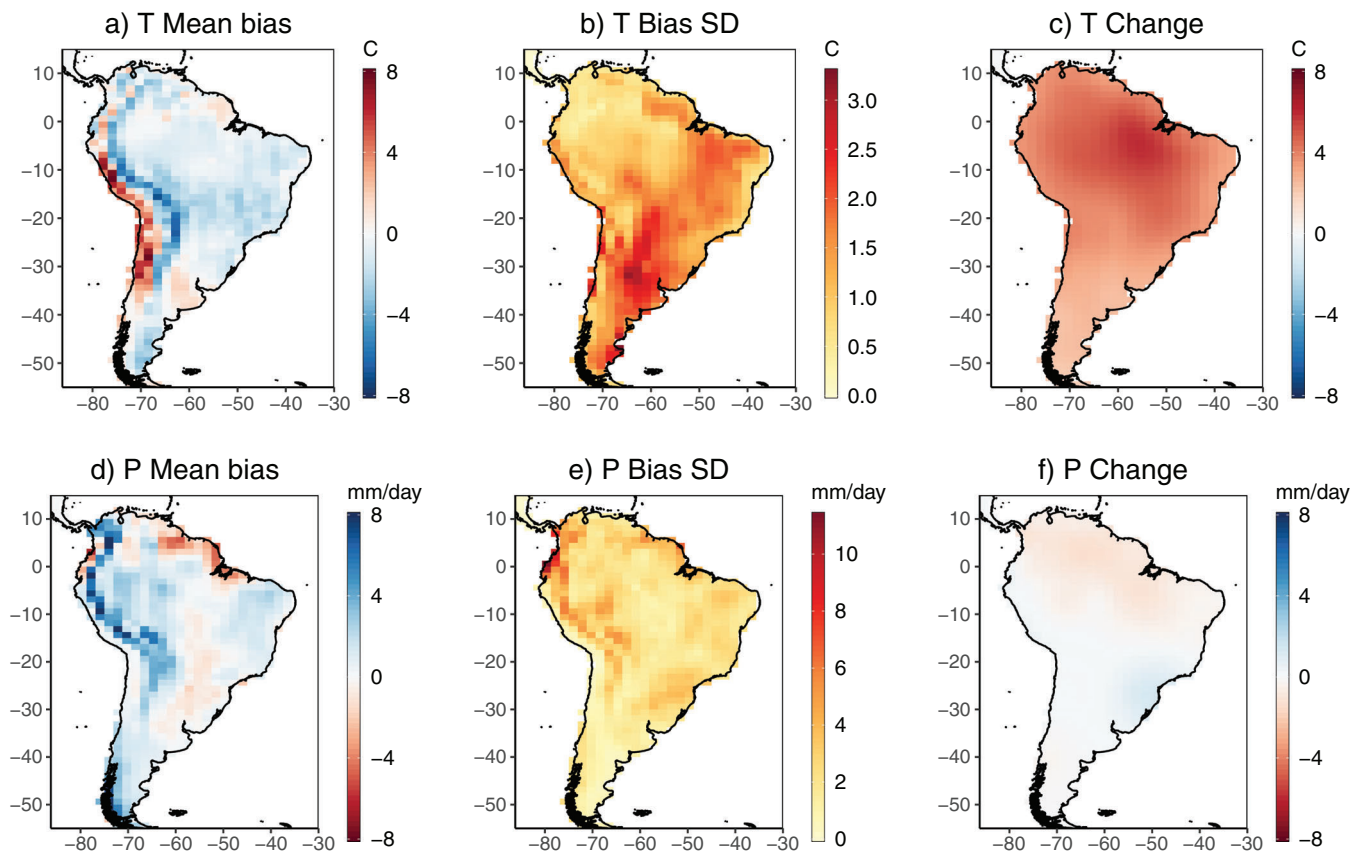
FIGURE 2 HadGEM2-ES biases and projections. Comparison of the magnitudes of bias correction versus climate change for near-surface temperature, T (first row), and for precipitation, P (second row). First column is annual mean offsets, as the average of the monthly bias corrections, shown as direct HadGEM2-ES diagnostics (i.e. without bias corrections) minus climatology based on CRU–JRA re-analysis values. The second column also relates to bias magnitude, and shows the standard deviations of the 12 bias correction values for each month and for each location. The third column presents the amount of annual mean climate change (future minus recent) between the recent past (mean of years 1999–2019) and towards the end of the 21st Century (2069–2089). We keep the colour bar ranges identical between the first and third columns for ease of comparison. Panels c and f are repeated in Figure S2 with colour bars more tightly aligned to the range of projected climate change

expected changes in the decades ahead (left and middle columns vs. right column of Figure 2). We also present annual biases, standard deviation of monthly corrections and the estimated changes in the other variables required to drive the JULES DGVM (Figure S1, same format as Figure 2). These extra quantities are humidity, downward shortwave and longwave radiation and windspeed, with the latter shown as mean zonal and meridional components. Biases are such that downward shortwave is too high across much of the Amazon suggesting the ESM projection of cloud cover is too low, whereas downward longwave is too low across the Amazon and the windspeeds are slightly too high. Under climate change, expected are increases in both downward shortwave radiation (implying a reduction in cloud cover) and humidity.

Returning to temperature and precipitation, in Figure S2 we compare the annual mean changes estimated by HadGEM2-ES, and under the RCP8.5 scenario, to those

of the mean of the models in the CMIP5 ensemble (Taylor et al., 2012). The HadGEM2-ES ESM warms by slightly more than the CMIP5 ensemble mean, and both estimate the highest warming levels are away from coastlines. The tendency of HadGEM2-ES to estimate lower future precipitation in Amazonia but increases in SE Brazil is also present in the mean of the CMIP5 simulations. Overall, the HadGEM2-ES ESM and CMIP5 ensemble mean estimates of temperature and precipitation changes are similar (Figure S2). To further illustrate the magnitude of our calculated offsets, we add the mean biases removed across South America (Section 2.1) back on to our future projections of temperature and precipitation (orange curves; Figure S3). The time series of annual mean values (Figure S3) is from averaging across the land points of Figure 2. Mean warming by the 2080s will be approximately 4°C above present day, whereas HadGEM2-ES is approximately 1°C too cold on average (Figure S3), although local and seasonal
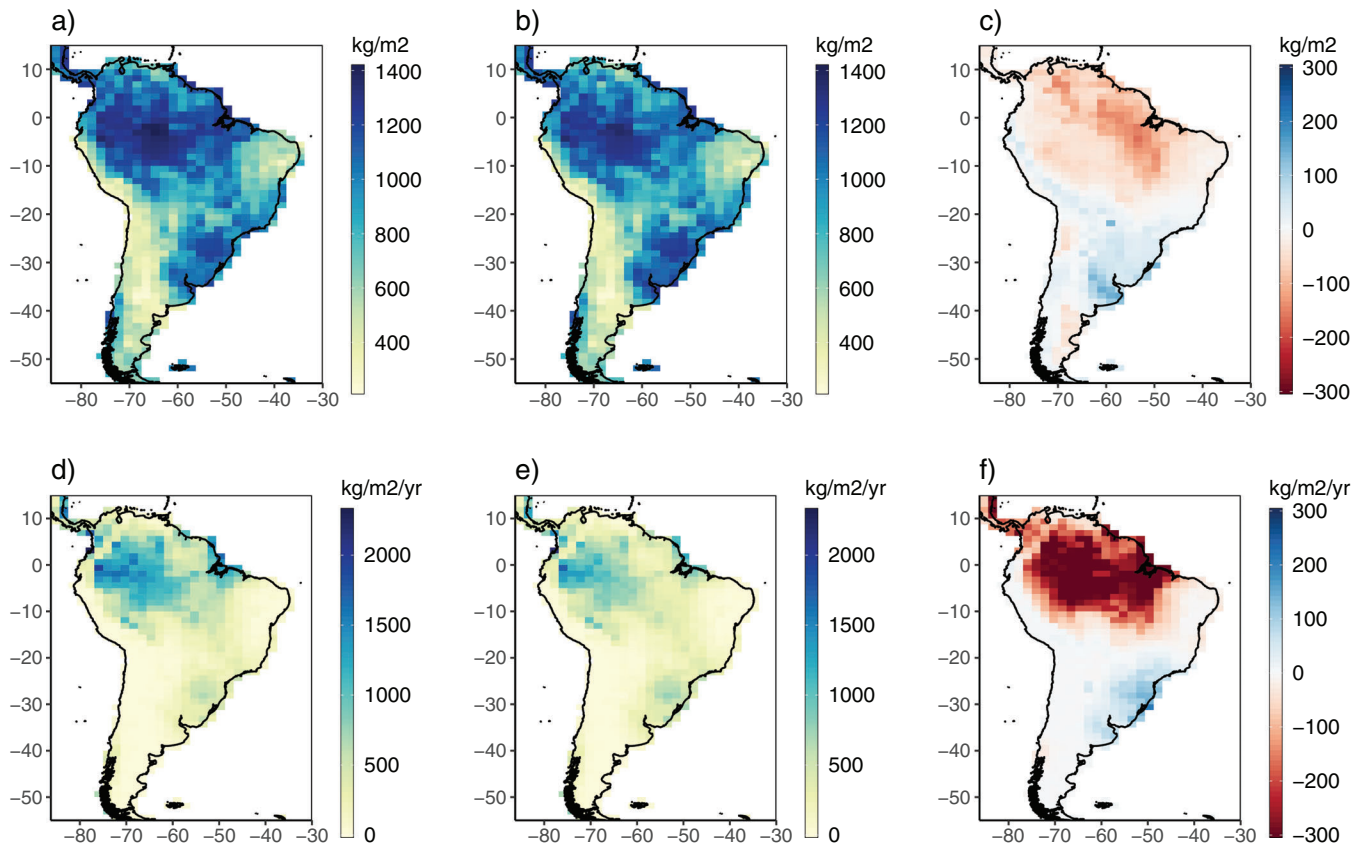
FIGURE 3 Hydrological variables. Spatial hydrological variables, and their changes, of soil moisture (top row) and surface runoff (bottom row). The left column is annual mean values, averaged for period 1999–2019, and the middle column is values for future period 2069–2089. The right column is the changes (future climate minus recent past, i.e. middle minus left columns)

differences may be larger (Figures 2a and 2b). For precipitation, Figure S3 reconfirms that across South America, the biases in precipitation are much larger than the expected changes during the 21st Century.

If land impacts respond linearly to climate change, biases propagate through transient climate–land simulations and so projected terrestrial changes remain trustworthy (even if the actual values have offsets). However, many land ecological responses have nonlinear responses to imposed near-surface meteorology. Hence, such responses depend on the absolute values of features of surface climate, such as temperature levels (e.g. Lloyd and Taylor, 1994; Kattge and Knorr, 2007; Mercado et al., 2018), suggesting the importance for ESM bias removal. Using linear 'pattern-scaling' (Huntingford and Cox, 2000) of projected climate changes by the HadCM3LC ESM, Huntingford et al. (2004) show that when combined with a DGVM, the prediction of Amazon 'dieback' depends on whether the estimated meteorological changes are added to the climate model pre-industrial state or the known climatology. In that analysis, removal of an initial dry bias lowered the projected risk of major land carbon store decreases. We now project future land surface responses to our new bias-

corrected data climate data, using the much more recent HadGEM2-ES ESM, and with a current version 5.4 of the JULES DGVM.

3.2 | Climate change impacts on future land biogeochemistry

Our focus is on climate change-induced variations to South America terrestrial carbon fluxes and their implications for carbon stores. These calculations are as estimated with the JULES DGVM (version 5.4) forced with projections from our bias-corrected ESM. However, carbon cycle changes link strongly to changes in the hydrological cycle, and so we first present projections of changes to soil moisture (Figure 3). With the strong societal implications of changing water-based attributes of the land surface, we also present estimates of runoff change (Figure 3). The most notable changes are the estimates of a general drying across much of North East Brazil, forcing the JULES model to project lower levels of soil moisture and runoff.

JULES broadly simulates an increase in NPP throughout this century (Figure 4a) in response to elevated
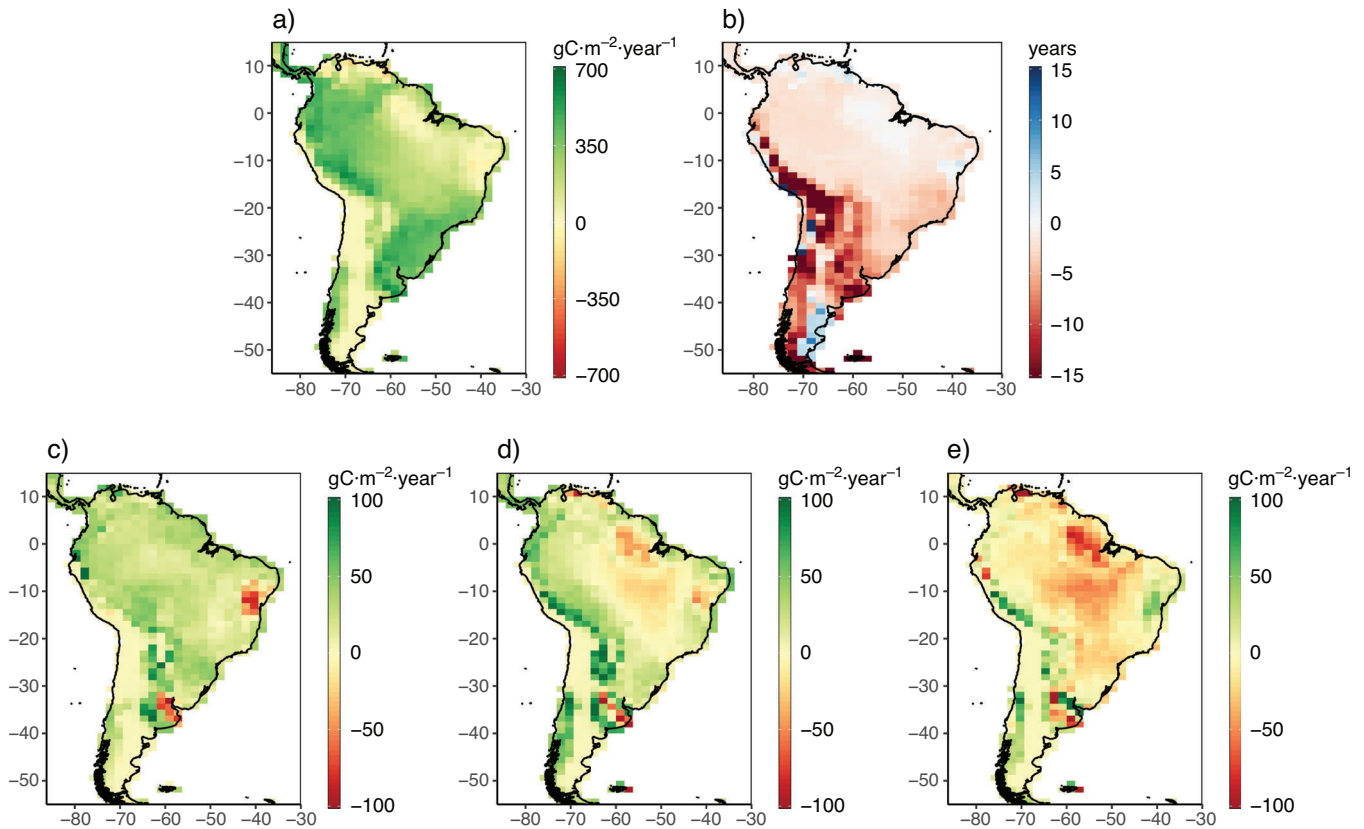
8 of 17

Climate Resilience and Sustainability
Interdisciplinary Approaches Towards Solutions for Climate Change   Open Access   ♦ **RMetS**

HUNTINGFORD ET AL.

FIGURE 4 Attributes of the South American terrestrial carbon cycle fluxes. Panel (a) is the change in NPP (period 2069–2089 minus 1999–2019) and (b) is the change in soil carbon residence time over the same timeframe. Panel (c) is NBP for period 1999–2019 and (d) is NBP for future period 2069–2089. Panel (e) is the projected NBP changes (middle minus left, lower plots). Negative values of NBP correspond to carbon released from the vegetation to the atmosphere. Values are gridbox means and are therefore calculated from the areal weighting based on PFT fractions

atmospheric CO_2 concentrations, outweighing any potential detrimental climate effects. The largest increase in NPP is simulated across the wet neotropical regions, that is the Atlantic forest region and western Amazonia. However, the increases are small or negligible in eastern Amazonia.

Soil carbon stores may alter under climate change. Cox et al. (2000) first identified the risk of diminishing soil stocks, although for that analysis the predicted losses occurred mainly in the mid-latitudes. Changes in soil carbon are a composite response of changing input, via litterfall (in turn, linked to NPP) and altered respiration outputs. Adjustments in microbial respiration rates are a response to climate, and to characterize this we calculate the residence time defined as soil carbon content divided by soil respiration rate (Figure 4b). For almost all of South America, there is a considerable reduction in soil residence time. Substantially lower residence times (i.e. raised turnovers) might counteract any higher incoming litterfall caused by more productive vegetation through fertilization, and so soil carbon stocks. Hence, in the lower panels of Figure 4, we first plot Net Biome Productivity (NBP), which is the overall net land atmosphere CO_2 flux of the combined

vegetation–soil system and is positive when the land surface is accumulating carbon (Figure 4, lower panels). As our model framework has invariant land use and no modelled fire, then NBP is identical to Net Ecosystem Exchange (NEE). For the mean period years 1999–2019, the majority of locations are sequestering carbon (Figure 4c). However, by 2069–2089 and for the RCP8.5 scenario, a substantial part of eastern Amazonia has become a net source, returning carbon to the atmosphere (Figure 4d). Across almost all the Amazonian region, there is a decrease in NBP towards the end of the 21st Century, compared to the recent past (Figure 4e). We present spatial maps of modelled changes in annual GPP in Figure S4, and this also shows much lower increases, or even decreases, for eastern Amazonia and over the same modelled period. There is also some suppression of autotrophic respiration in the same locations (Figure S4).

We investigate the substantial decreases in NBP compared to the contemporary period (and that sometimes become negative) by studying the estimated changes to vegetation and soil carbon stocks. Tree cover is projected to expand at most locations (Figure 5a), and related to this
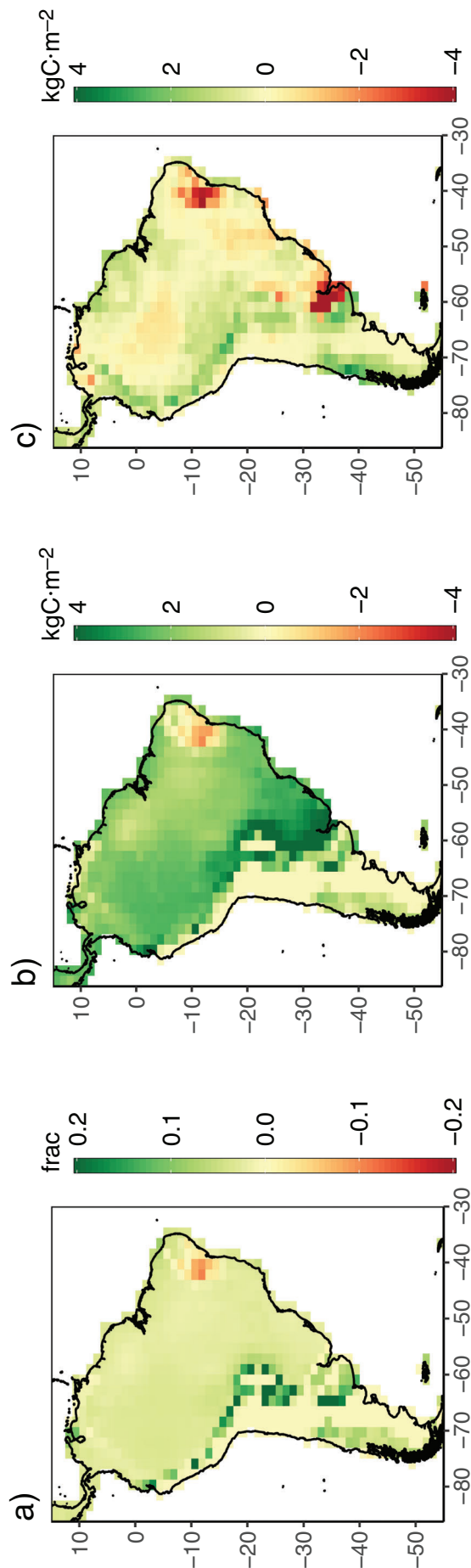
FIGURE 5 Attributes of the South American terrestrial carbon stocks. Changes in panel (a) tree fraction, (b) vegetation carbon and (c) soil carbon. Values presented for each quantity are the average of annual mean values for period years 2069–2089 minus 1999–2019. Panels (b) and (c) are gridbox means and therefore calculated from the areal weighting based on PFT fractions

is that vegetation carbon will increase almost everywhere (Figure 5b). For soil carbon, the changes are more heterogeneous, and noting in particular that there are parts of Amazonia where soil carbon stores will be less than the recent past. We interpret aspects of Figures 4 and 5 together as follows. As NPP generally increases (Figure 4a) yet NBP decreases in many regions (Figure 4e), this implies that soil respiration increases more than NPP by the end of the 21st Century and compared to the present day. High contemporary values of NPP could mean that despite the large soil respiration changes, this can still result in NPP being higher than soil respiration by the end of the 21st Century and so NBP remains positive. However, in most of Amazonia, NBP changes from being positive to negative, and so increases in soil respiration are even more substantial and overtake the absolute value of NPP (thus including its rises) by the end of our simulations. Negative NBP by the end of this century (Figure 4d) is in keeping with the decreasing soil carbon residence times (Figure 4b), causing the land to switch to losing carbon to the atmosphere.

Despite our finding of widespread decreasing soil carbon stocks towards the end of this century, at many locations, soil carbon content still increases between now and that future time (Figure 5c). This implies that soil carbon stocks for much of South America will initially increase, peak and then start to decrease as temperature-induced respiration rises outpace incoming litterfall. A summary, therefore, is that the Amazon will have a more productive and resilient forest (Figure 5a,b) but because of enhanced soil microbial activity, it will transition in some locations to a carbon source to the atmosphere (Figure 5c).

To confirm our broad interpretation of the maps of terrestrial carbon fluxes and stores, and their changes (Figures 4 and 5), we present the projected time series of area-averaged land changes for the same region driven by our bias-corrected ESM. These are the black curves for recent past, followed by blue curves for future projections in Figure 6. The orange curves of Figure 6 are with the removed monthly biases re-added to the bias-corrected simulations, and so approximate using HadGEM2-ES ESM forcings directly. Both soil moisture and runoff are projected to have a steady decline across South America (Figure 6a,b). There is a broad increase in NPP as CO_2 rises (Figure 6c), and with the rise slightly more substantial for the uncorrected ESM data (orange curves). Soil carbon residence times decrease (Figure 6d). Notably, NBP decreases (Figure 6e) towards the end of the simulations, and there are multiple years with negative values, illustrating some consistency with Figure 4d. Soil respiration changes are given in Figure 6f. For both simulations, soil respiration rises in time, and as for NPP, the magnitudes of increase are slightly more for the response to non-bias-corrected
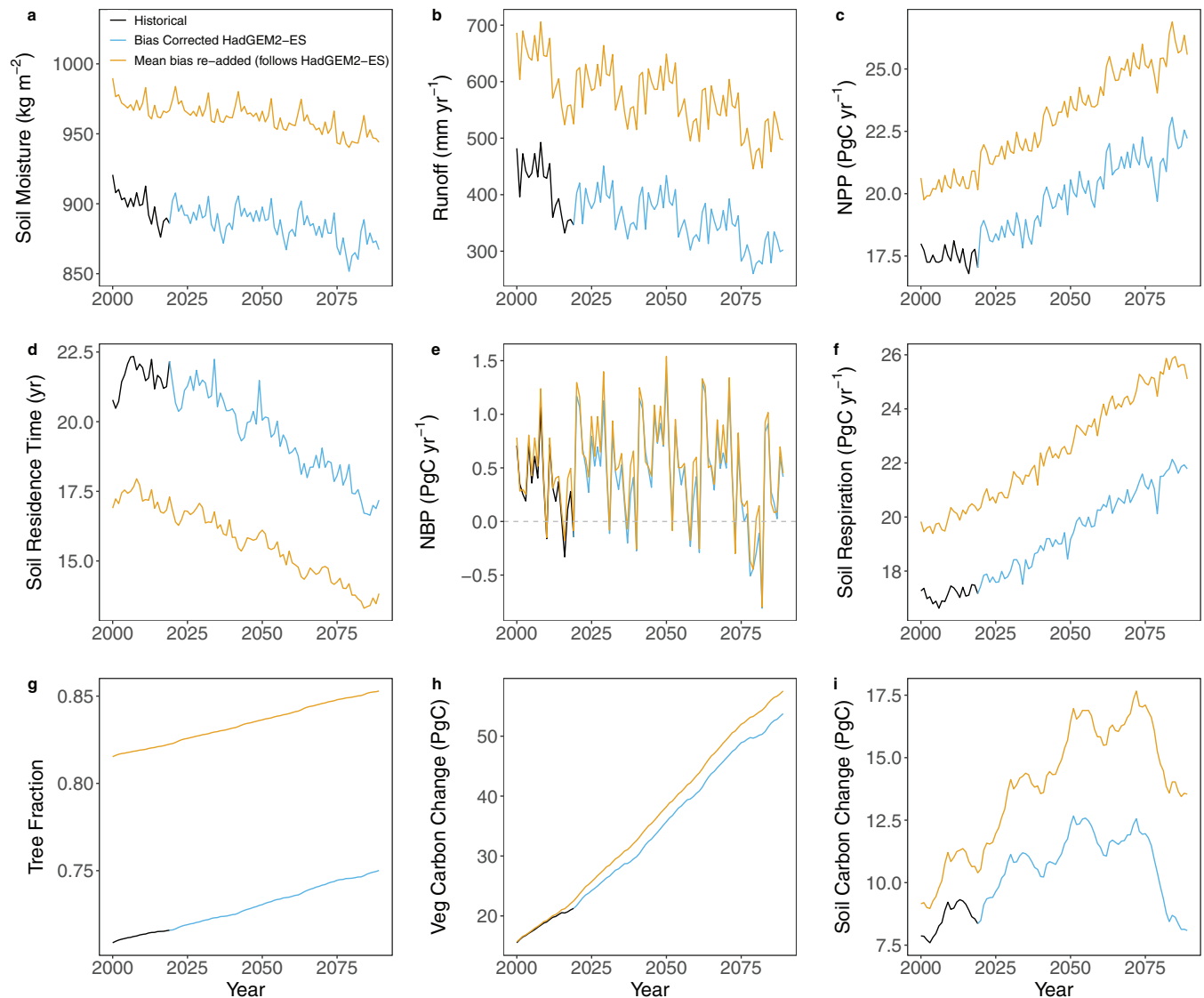
FIGURE 6 Time series of South American land changes for the RCP8.5 greenhouse gas scenario. Time-evolving annual values of spatially averaged attributes of the land for South America (areal averages across same domain as the maps of Figures 2–5). Spatial means are for the hydrological variables of (a) soil moisture and (b) runoff, and of carbon-related variables of (c) net primary productivity, (d) soil carbon residence time, (e) net biophysical production, (f) soil respiration, (g) tree fraction, (h) vegetation carbon and (i) soil carbon. The black and blue curves are simulated land changes when forced with historical measurement-based data from the CRU–JRA data set, followed by our bias-corrected version of the HadGEM2-ES ESM. The orange curves are for forcing where the mean monthly ESM bias corrections are added back on to the historical and corrected future data. This approach to reintroducing biases ensures that the emphasis is on the mean offset errors, while retaining similarities for the higher frequency variations contained in the drivers needed by the JULES DGVM. All calculations are from year 1901, but to aid focus on the decades ahead, presented are years from 1990 onwards only. Panels (h) and (i) are anomalies, relative to period 1901–1930

climate drivers. For the carbon stores, tree fraction increases in a near-linear fashion, and additionally so does vegetation carbon (Figure 6g,h).

The time series showing the most substantial difference between the response to climate drivers, with and without bias correction, is for soil carbon (Figure 6i). Our bias-corrected simulations project an initial increase, followed by a decrease in soil carbon, and this matches our interpretation above of Figures 4 and 5. That is, the blue curve of

Figure 6i first rises, but then falls such that by towards the end of the 21st Century, South American soils are returning CO_2 to the atmosphere. This response contrasts to soil stocks modelled for the ESM-based forcing without bias removal, where there is an increase up to a higher peak around year 2075 (orange curve, Figure 6i). By the end of simulations at modelled year 2089, the projections with bias removal estimate approximately 5 GtC less vegetation carbon change and 7 GtC less soil carbon change across
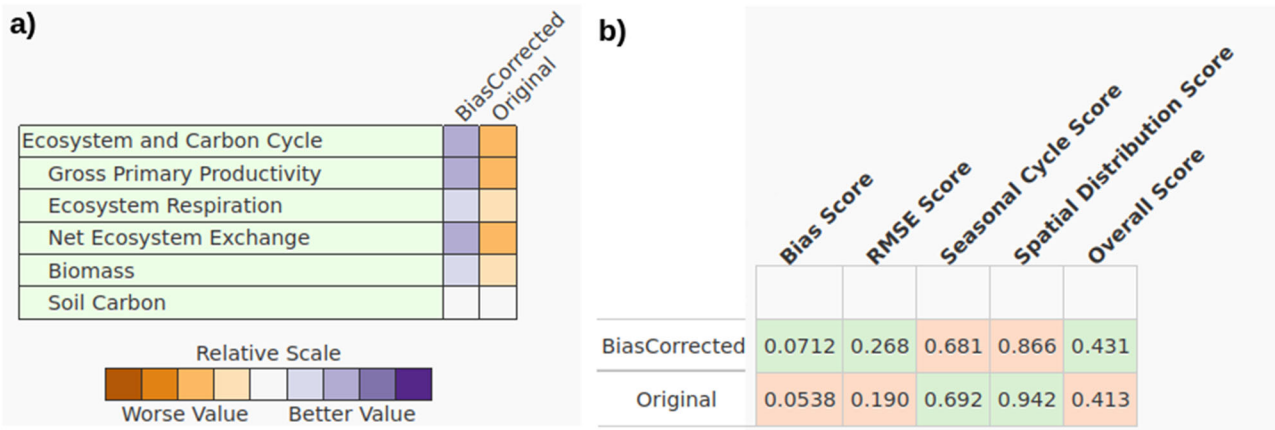
HUNTINGFORD ET AL.

Climate Resilience and Sustainability
Interdisciplinary Approaches Towards Solutions for Climate Change · Open Access

RMetS | **11 of 17**

FIGURE 7 ILAMB statistics. (a) Comparison of the relative performance of JULES-ES forced by bias-corrected climate data from HadGEM2-ES (marked here as 'BiasCorrected') and with mean biases re-added to the climate forcing data ('Original'). Calculations are for South America, obtained by placing JULES-ES projections in the International Land Model Benchmarking system (ILAMB) framework and selecting the comparison against the GBAF/FLUXCOM gridded data. As the DGVM data examined are for the recent historical period, the climate forcing data used in our simulations that we describe as bias-corrected are that of the CRU–JRA data set. (b) Statistics for the performance of both sets of simulations at projecting ecosystem respiration (Collier et al., 2018 for details). It is the overall bias score in panel (a) that determines the colour coding for ecosystem respiration in panel (a)

South America compared to no bias correction (Figures 6h and 6i, respectively).

In a final comparison of the effects of bias correction, we test our two configurations of HadGEM2-ES forcing JULES (i.e. with and without bias-correcting) in the International Land Model Benchmarking (ILAMB) framework (Collier et al., 2018). We derive relative values of performance for South America, and for key carbon-related land surface attributes (Figure 7). JULES-ES forced with bias-corrected data performs better than using HadGEM2-ES outputs without bias removal for all quantities, although for overall ecosystem respiration (plant plus soil), the difference is marginal (Figure 7a; 'overall score' statistic, Figure 7b). As our analysis is for all of South America, we select the ILAMB version where estimates of ecosystem respiration are based solely on GBAF/FLUXCOM gridded data (Jung et al., 2020), and therefore does not contain additional direct comparison to eddy covariance measurements. GBAF/FLUXCOM are, though, informed by FLUXNET (e.g. Baldocchi, 2008) eddy covariance sites, of which there are six in South America (Jung et al., 2010; Figure S1). When looking at individual statistics (Collier et al., 2018) for ecosystem respiration (Figure 7b), our calculations without bias correction perform better in simulating the seasonal cycle and spatial distribution of respiration across South America. The full suite of ILAMB diagnostics, for both simulations and all five ecosystem and carbon cycle variables listed in Figure 7b, is available in a directory in the Supporting Information. We note again that for our simulations named as bias-corrected (Section 2.2), for the recent past and hence the period of

ILAMB comparison, these calculations use the CRU–JRA gridded climate forcing directly.

4 | DISCUSSION

A drying is projected for eastern Amazonia, based on the HadGEM2-ES ESM (Figure 3c,f). This lower water availability aligns with evidence in the measurement record of recent drying in eastern Amazonia (Esquivel-Muelbert et al., 2019). Such drying, although in tandem with land use change, is believed to have already started turning eastern Amazonia into a source of CO_2 to the atmosphere (Gatti et al., 2021). Elsewhere in mid- and southern South America, model estimates are of small increases in soil moisture and runoff. Rising atmospheric CO_2 leads to a fertilization that increases plant productivity by enhancing photosynthesis and also increases water-use efficiency. Hence in many circumstances, changing CO_2-driven effects can offset any detrimental impacts of warming or declines in precipitation. Warming does, though, act to directly affect physiological rates of photosynthesis, with the potential to exceed optimum rates. Warming also raises atmospheric demand through potential evapotranspiration, which in tandem with any reductions in precipitation leads towards drought that can then suppress NPP. Hence, in eastern Amazonia, there is little simulated change in NPP over this century (Figure 4a), in keeping with the hydrological findings of Figure 3. Hence, for that location, reductions in precipitation and substantial warming (Figure 2c) strongly offset the CO_2 fertilization effect.

12 of 17

Climate Resilience and Sustainability
Interdisciplinary Approaches Towards Solutions for Climate Change
Open Access RMetS

HUNTINGFORD ET AL.

There is potential for soil carbon stocks to decrease under global warming. Such decreases act as a positive feedback on climate (Cox et al., 2000), although for that analysis soil carbon stock changes are projected mainly in the mid-latitudes. Changes in soil carbon are a composite response of changing input, via vegetation litterfall that in turn links to any CO_2-induced rises in NPP, and output via increasing soil respiration losses under global warming. To characterize alterations in microbial respiration rates, we analyse the modelled evolution to the residence time of soil carbon (Figure 4b), estimated as instantaneous soil carbon content divided by soil respiration rate. For almost all South America, there is a considerable reduction in soil residence time through temperature-induced raised microbial activity. Notable is a recent warming experiment of tropical soils (in Panama) revealing they are likely to be highly sensitive to rises in temperature (Nottingham et al., 2020). Any projected transition of soils to a source of CO_2 under global warming will be sensitive to the modelled temperature response. Here, the simulated soil respiration follows a Q_{10} profile, which with a value of 2 and with all other factors equal, would be a doubling for a rise in temperature of 10°C. An alternative description is that of Lloyd and Taylor (1994) or the RothC soil model (Jenkinson, 1990), which have a more amplified respiration rate at low temperatures, and more damping at high temperatures compared to the Q_{10} description (for a comparison of thermal response functions, see Jones et al., 2005). Models representing carbon–nitrogen dynamics typically simulate an increase in N mineralization with warming, potentially affecting respiration in high latitudes. This is less relevant in tropical ecosystems, which have old, highly weathered tropical soils, and where the controlling nutrient is phosphorus. Understanding and modelling the tropical phosphorus cycle, for eventual placement in global models, is an active area of current research (Yang et al., 2016; Fleischer et al., 2019; Sun et al., 2021).

As raised soil respiration might counteract any higher NPP and thus incoming litterfall, we also place an emphasis on NBP and its changes (Figure 4c–e). NBP is especially important as this quantity defines the overall net land–atmosphere CO_2 flux of the combined vegetation–soil system. For the recent past, the majority of South America has sequestered carbon (i.e. positive NBP values), contributing to the natural partial offset of anthropogenic CO_2 emissions. However, by period 2069–2089 and for the RCP8.5 forcing scenario, a substantial part of the modelled Amazon basin has become a net source (Figure 4d), returning carbon to the atmosphere. This change to a source is especially in eastern Amazonia, where there are large decreases in soil moisture (Figure 3c) and the suppression of NPP rise. Over almost all the Amazonian region, there is a decrease in NBP towards the end of the 21st Century,

compared to the recent past (Figure 4e). Our interpretation of these projections is that NPP rises, and so increases litterfall, but these are overtaken by soil respiration losses. The size of this balance for soils is such that by the end of the 21st Century, in some locations the magnitude of time-evolving rate of vegetation carbon stock increases is smaller than that of soil carbon stock decreases, causing the negative NBP values. Soil carbon losses are sufficiently large that in some locations, for example eastern Amazonia, soil carbon stocks are smaller by the period 2069–2089 compared to 1999–2019 (Figure 5c). These effects are supported by Figure 6i (black and blue curve), which shows that when averaged across South America, soil carbon stocks increase to the middle of the 21st Century, followed by decreases back to present-day levels. As noted in Section 3.2, for driving data that is not bias-corrected (orange curve), soil carbon stocks instead increase much more in the next few decades ahead (Figure 6i). The non-bias-corrected calculation has a slightly later peak, and higher soil carbon values for the end of simulations at year 2089 (Figure 6i).

Changes to forests impact vegetation carbon stocks as well as soil carbon stocks via litterfall. Determining the risk of Amazon rainforest 'die-back' remains a key scientific challenge. A temperature rise of ~4°C and above, as in our RCP8.5 simulation, may represent a breakpoint in biogeochemical response to climate warming (Johnston et al., 2021). Given the hypothesis that tropical forests have narrow temperature ranges due to long-term adaptation to a stable thermal environment (Mercado et al., 2018), this emphasizes the need for bias-corrected forcing. Overall, our model structure suggests enhancements in vegetation productivity in South America this century, despite warmings reaching order ~4°C. Hence, CO_2 fertilization will offset possible deleterious effects of warming (see figure 6.22 of Ciais et al., 2013, p. 522). Where productivity declines are simulated towards the end of the 21st Century, this is in eastern Amazonia, and are due to the combined effects of warming and drought. These findings, for tropical forests, match evidence from multiple sources (Lewis et al., 2009), and from other DGVMs for South America (Sitch et al., 2015). There are similarities between the JULES model (and in particular the TRIFFID component; Cox, 2001) and other DGVMs. Such similarities include their responses to CO_2 rise and the individual components of meteorological change for Amazonia (Galbraith et al., 2010). An overall comparison of DGVM responses with early generation models, but including TRIFFID, is by Sitch et al. (2008).

Theoretically, one expects the warm tropical regions to benefit most from elevated CO_2, although this remains untested empirically (Hickler et al., 2008). Productivity enhancements may, though, become increasingly limited by nutrient constraints, and in particular phosphorus in

HUNTINGFORD ET AL.

Climate Resilience and Sustainability
Interdisciplinary Approaches Towards Solutions for Climate Change · Open Access · RMetS · 13 of 17

old, weathered tropical soils (Vitousek, 1984; Quesada et al., 2012). A multi-model study projects a 50% reduction in biomass carbon growth under elevated CO_2 with including phosphorus constraints (Fleischer et al., 2019), although these results also require empirical confirmation. Wang and Goll (2021) argue that where there are major gaps in the understanding of terrestrial nutrient cycle, some may be closed under the application of appropriate optimality assumptions. Wang and Goll (2021) also advise the use of machine learning methods to relate spatially diverse measurements of nutrient interactions in ecosystems to DGVMs, as similarly suggested by Huntingford et al. (2019). A caveat of our analysis, therefore, is as these nutrient processes are presently missing in the JULES DGVM, their incorporation may cause revisions of lower projected NPP and therefore litterfall.

There are other caveats associated with missing processes in the JULES DGVM. Studies on intact forests indicate a diminishing Amazon carbon sink as mortality rates are increasing faster under warming than (and therefore catching up with) productivity increases (Brienen et al., 2015; Hubau et al., 2020). Although DGVMs have a detailed representation of short-term fluxes and coupled photosynthesis and water cycles, they often omit detailed representations of plant hydraulics and mortality processes in a single common framework. These omissions are now areas of active development. The recent availability of data on plant traits and hydraulics, combined with advancement in hydraulic theory, has enabled new parsimonious approaches to model such processes at the global scale (e.g. Anderegg and Venturas, 2020; Eller et al., 2020; Wang et al., 2020). These developments will align with a parallel growing understanding of the role of non-structural carbohydrates (e.g. Jones et al., 2020). Such knowledge will allow the exploration of alternative hypotheses to current modelling based on describing carbon sources via NPP and instead towards a direct growth-based approach. Such advances may include a move from only simulating source activity (i.e. photosynthesis) to a modelling paradigm of the formal representation of growth activity (i.e. via tissue growth) (Korner, 2015).

Next-generation DGVMs strive to include an explicit representation of ecosystem demography and disturbance (e.g. Moore et al., 2018; Burton et al., 2019; Argles et al., 2020; Moore et al., 2020). Estimates by the JULES model of vegetation and soil carbon are routinely validated against satellite measurements (e.g. figure 18 of Sellar et al., 2019). Future comparisons against such data will provide verification of the aggregated performance of any inclusion of ecosystem demography components. As satellite records extend in time, this opens the possibility to constrain trends projected by demography components, in addition to background mean values. The use of satellite data has

also identified the vegetation state of previous seasons as influencing natural fire risk (Forkel et al., 2019), suggesting that adding fire modules to DGVMs requires the simultaneous introduction of more advanced representation of vegetation structure. In the coming years, the modelling community will be well-placed to combine these separate development strands, in parallel with simulating the extensive disturbance by deliberate deforestation across the Amazon that our study omits. Better data-led estimates of diffuse radiation levels may account for its modulation by deliberate land disturbance by fires and the smoke they place in the atmosphere. This alteration of diffuse radiation, due to fires, feeds back on vegetation productivity, as modelled with an ESM (Malavelle et al., 2019), or studied with machine learning methods to capture the specific complexities of Amazonian forest canopies (Braghiere et al., 2020a). Refined estimates of light interception may include any specific effects of vegetation clumping within canopies and the resultant influence on GPP (e.g. Braghiere et al., 2019). Modelled light interception, with a diffusive component, at two Amazon sites illustrates a strong dependence of GPP on metrics of clumping (Braghiere et al., 2020b; Figure 4). We note the review of the effectiveness of two-stream canopy radiative transfer models, and its potential for enhancement (Yuan et al., 2017). Determining the precise impact of elevated CO_2 on tropical forests needs empirical evidence from experimental programmes such as AmazonFACE, allowing the testing and calibration of DGVMs in ways similar to current assessments in non-tropical regions (e.g. Liu et al., 2019). Such understanding must also capture nutrient limitation effects (e.g. Fleischer et al., 2019; Terrer et al., 2019), and a recently developed version of JULES with a nitrogen cycle ('JULES-CN') is currently being tested for its performance (Wiltshire et al., 2021).

Our paper primarily identifies the risk of South America soils changing from a carbon sink to a source due to higher soil respiration under global warming. However, required is the constraining of understanding of above-ground productivity, because this impacts the level of litterfall into the soil carbon stores. Recent tests (Friedlingstein et al., 2019; Appendix B, Figure B2) include passing our JULES DGVM (version JULES-ES) through the International Land Model Benchmarking system (ILAMB; Collier et al., 2018). Globally, JULES-ES performs well compared to other DGVMs for contemporary projections of soil carbon, overall respiration and NEE. However, we urge retesting in ILAMB any new model versions that incorporate the proposed missing processes described above, to check if performance improves further. We particularly note the inconclusive assessment of whether estimated overall ecosystem respiration with JULES-ES is better simulated with or without our bias-corrected climate driving data, depending on the

14 of 17

Climate Resilience and Sustainability
Interdisciplinary Approaches Towards Solutions for Climate Change
Open Access · RMetS

HUNTINGFORD ET AL.

statistic considered. The relatively small number of eddy covariance measurements available to inform ILAMB for South America is also noted. Many researchers (e.g. Hill et al., 2016) highlight the need for more eddy covariance sampling, and including potential replication at similar locations, to lower uncertainty. The debate continues on how representative the footprint of a single eddy covariance site might be (Chu et al., 2021), which is important when using such data to calibrate or test large-scale land models. There is also a challenge with the use of flux data in separating the net flux into the gross component fluxes, because the unaccounted processes of inhibition of leaf respiration in the light could lead to biases up to 25% (Keenan et al., 2019).

5 | CONCLUSIONS

Our focus is on bias-correcting the HadGEM2-ES ESM and using such data to force the JULES DGVM to estimate terrestrial carbon flux and store changes across South America and over the 21st Century. The motivation for ESM bias removal is noting that many researchers identify the Amazon forest as having a potential tipping point in response to climate change (e.g. Drijfhout et al., 2015). Tipping points are nonlinear by definition and so depend on the absolute value of any forcing components. Our ESM bias correction is by normalization to the CRU–JRA gridded estimates of climate during recent decades. We apply the derived offsets to a future HadGEM2-ES projection that corresponds to the RCP8.5 scenario. We find that climate-enhanced faster turnover of soil carbon translates into an ∼30% increase in microbial respiration rates for a continental-scale warming of 4°C, which is similar to the data-led extrapolation by Nottingham et al. (2020) for tropical forests. NPP also increases, and this will raise litterfall as atmospheric CO_2 rises, but in many locations this enhancement is insufficient to prevent soil carbon stores from decreasing by the end of the 21st Century through respiration losses. Further, in some locations, these decreasing soil carbon stores are large enough to cause NBP to become negative, despite a modelled resilient forest and corresponding increase in vegetation carbon stores. Negative NBP acts as a positive feedback to the effects of a changing climate, by the land returning CO_2 to the atmosphere. Some authors find evidence of a decreasing South American carbon sink in recent measurements (e.g. Gloor et al., 2012). Of note is that when using the non-bias-corrected driving data, this also projects soil carbon to peak before becoming a source under RCP8.5. However, this peak occurs later under RCP8.5, and the soil store size does not fall back to contemporary levels by the 2080s, compared to calculations with the bias-corrected climate forcings.

In summary, for the RCP8.5 GHG scenario and bias-corrected drivers based on the HadGEM2-ES ESM driving the JULES DGVM, much of the modelled Amazon transitions from a land carbon sink towards a source over this century due to climate change. This finding is from a warming-induced stimulation of soil microbial activity, a frequently overlooked aspect of tropical forest biogeochemistry. We illustrate that bias-correcting a climate model can impact substantially future projections of the evolution of South American terrestrial carbon stocks.

DATA AVAILABILITY STATEMENT
The CRU–JRA data set is available from the CEDA archive of atmospheric data. The HadGEM2-ES climate model is available as one of the CMIP5 models, held by the portal of the Earth System Grid Federation. The code of the JULES model is held at jules.jchmr.org, and its outputs that inform Figures 3–7 and Figure S4 are available upon request from the authors.

CONFLICT OF INTEREST
The authors declare no conflict of interest.

PERMISSIONS
The manuscript uses no material from other resources for which permission to reproduce is required.

ORCID
Chris Huntingford https://orcid.org/0000-0002-5941-7770
Stephen A. Sitch https://orcid.org/0000-0003-1821-8561
Michael O'Sullivan https://orcid.org/0000-0002-6278-3392

REFERENCES
Anderegg W.R.L. & Venturas M.D. (2020) Plant hydraulics play a critical role in Earth system fluxes. *New Phytologist*, 226(6), 1535–1538.

Argles A.P.K., Moore J.R., Huntingford C., Wiltshire A.J., Harper A.B., Jones C.D., et al. (2020) Robust Ecosystem Demography (RED version 1.0): A parsimonious approach to modelling vegetation dynamics in Earth system models. *Geoscientific Model Development*, 13(9), 4067–4089.

Baldocchi D. (2008) Breathing of the terrestrial biosphere: Lessons learned from a global network of carbon dioxide flux measurement systems. *Australian Journal of Botany*, 56(1), 1–26.

HUNTINGFORD ET AL.

Climate Resilience and Sustainability
Interdisciplinary Approaches Towards Solutions for Climate Change Open Access RMetS | 15 of 17

Best M.J., Pryor M., Clark D.B., Rooney G.G., Essery R.L.H., Ménard C.B., et al. (2011) The Joint UK Land Environment Simulator (JULES), model description - Part 1: Energy and water fluxes. *Geoscientific Model Development*, 4(3), 677–699.

Booth B.B.B., Jones C.D., Collins M., Totterdell I.J., Cox P.M., Sitch S., et al. (2012) High sensitivity of future global warming to land carbon cycle processes. *Environmental Research Letters*, 7(2), 024002.

Braghiere R.K., Yamasoe M.A., Évora Do Rosário N.M., Ribeiro Da Rocha H., De Souza Nogueira J. & De Araújo A.C. (2020a) Characterization of the radiative impact of aerosols on CO_2 and energy fluxes in the Amazon deforestation arch using artificial neural networks. *Atmospheric Chemistry and Physics*, 20(6), 3439–3458.

Braghiere R.K., Quaife T., Black E., Ryu Y., Chen Q., De Kauwe M.G., et al. (2020b) Influence of sun zenith angle on canopy clumping and the resulting impacts on photosynthesis. *Agricultural and Forest Meteorology*, 291, 108065.

Braghiere R.K., Quaife T., Black E., He L. & Chen J.M. (2019) Underestimation of global photosynthesis in earth system models due to representation of vegetation structure. *Global Biogeochemical Cycles*, 33, 1358–1369.

Brienen R.J.W., Phillips O.L., Feldpausch T.R., Gloor E., Baker T.R., Lloyd J., et al. (2015) Long-term decline of the Amazon carbon sink. *Nature*, 519(7543), 344-348.

Burton C., Betts R., Cardoso M., Feldpausch T.R., Harper A., Jones C.D, et al. (2019) Representation of fire, land-use change and vegetation dynamics in the Joint UK Land Environment Simulator vn4.9 (JULES). *Geoscientific Model Development*, 12(1), 179–193.

Chu H., Luo X., Ouyang Z., Chan W.S., Dengel S., Biraud S.C.., et al. (2021) Representativeness of Eddy-Covariance flux footprints for areas surrounding AmeriFlux sites. *Agricultural and Forest Meteorology*, 301–302, 108350

Ciais P., Sabine C., Bala G., Bopp L., Brovkin V., Canadell J., et al. (2013) Carbon and other biogeochemical cycles. In: T.F. Stocker, D. Qin, G.-K. Plattner, M. Tignor, S.K. Allen, J. Boschung, et al. (Editors), *Climate change 2013: The physical science basis. Contribution of Working Group I to the Fifth Assessment Report of the Intergovernmental Panel on Climate Change.* Cambridge, UK and New York, NY: Cambridge University Press, pp. 465–570.

Clark D.B., Mercado L.M., Sitch S., Jones C.D., Gedney N., Best M.J., et al. (2011) The Joint UK Land Environment Simulator (JULES), model description - Part 2: Carbon fluxes and vegetation dynamics. *Geoscientific Model Development*, 4(3), 701–722.

Collier N., Hoffman F.M., Lawrence D.M., Keppel-Aleks G., Koven C.D., Riley W.J., et al. (2018) The International Land Model Benchmarking (ILAMB) system: Design, theory, and implementation. *Journal of Advances in Modeling Earth Systems*, 10(11), 2731–2754.

Cox P. (2001) Description of the "TRIFFID" dynamic global vegetation model. Hadley Centre Technical Note 24. Bracknell, UK: Hadley Centre, Met Office.

Cox P.M., Betts R.A., Jones C.D., Spall S.A. & Totterdell I.J. (2000) Acceleration of global warming due to carbon-cycle feedbacks in a coupled climate model. *Nature*, 408(6809), 184–187.

Drijfhout S., Bathiany S., Beaulieu C., Brovkin V., Claussen M., Huntingford C., et al. (2015) Catalogue of abrupt shifts in Intergovernmental Panel on Climate Change climate models. *Proceedings of the National Academy of Sciences of the United States of America*, 112(43), E5777-E5786.

Duffy K.A., Schwalm C.R., Arcus V.L., Koch G.W., Liang L.L. & Schipper L.A. (2021) How close are we to the temperature tipping point of the terrestrial biosphere? *Science Advances*, 7(3), eaay1052.

Eller C.B., Rowland L., Mencuccini M., Rosas T., Williams K., Harper A., et al. (2020) Stomatal optimization based on xylem hydraulics (SOX) improves land surface model simulation of vegetation responses to climate. *New Phytologist*, 226(6), 1622–1637.

Esquivel-Muelbert A., Baker T.R., Dexter K.G., Lewis S.L., Brienen R.J.W., Feldpausch T.R., et al. (2019) Compositional response of Amazon forests to climate change. *Global Change Biology*, 25(1), 39–56.

Fleischer K., Rammig A., De Kauwe M.G., Walker A.P., Domingues T.F., Fuchslueger L., et al. (2019) Amazon forest response to CO2 fertilization dependent on plant phosphorus acquisition. *Nature Geoscience*, 12(9), 736-741.

Forkel M., Andela N., Harrison S.P., Lasslop G., Van Marle M., Chuvieco E., et al. (2019) Emergent relationships with respect to burned area in global satellite observations and fire-enabled vegetation models. *Biogeosciences*, 16, 57–76.

Friedlingstein P., Jones M.W., O'sullivan M., Andrew R.M., Hauck J., Peters G.P., et al. (2019) Global Carbon Budget 2019. *Earth System Science Data*, 11(4), 1783–1838.

Friedlingstein P., O'sullivan M., Jones M.W., Andrew R.M., Hauck J., Olsen A., et al. (2020) Global Carbon Budget 2020. *Earth System Science Data*, 12(4), 3269–3340.

Galbraith D., Levy P.E., Sitch S., Huntingford C., Cox P., Williams M., et al. (2010) Multiple mechanisms of Amazonian forest biomass losses in three dynamic global vegetation models under climate change. *New Phytologist*, 187, 647–665.

Gatti L.V., Basso L.S., Miller J.B., Gloor M., Gatti Domingues L., Cassol H.L.G., et al. (2021) Amazonia as a carbon source linked to deforestation and climate change. *Nature*, 595, 388–393.

Gloor M., Gatti L., Brienen R., Feldpausch T.R., Phillips O.L., Miller J., et al. (2012) The carbon balance of South America: A review of the status, decadal trends and main determinants. *Biogeosciences*, 9, 5407–5430.

Harper A.B., Cox P.M., Friedlingstein P., Wiltshire A.J., Jones C.D., Sitch S., et al. (2016) Improved representation of plant functional types and physiology in the Joint UK Land Environment Simulator (JULES v4.2) using plant trait information. *Geoscientific Model Development*, 9(7), 2415–2440.

Harper A.B., Wiltshire A.J., Cox P.M., Friedlingstein P., Jones C.D., Mercado L.M., et al. (2018) Vegetation distribution and terrestrial carbon cycle in a carbon cycle configuration of JULES4.6 with new plant functional types. *Geoscientific Model Development*, 11(7), 2857–2873.

Harris I., Jones P.D., Osborn T.J. & Lister D.H. (2014) Updated high-resolution grids of monthly climatic observations – The CRU TS3.10 dataset. *International Journal of Climatology*, 34(3), 623–642.

Harris I.C. (2019a) *A forcings dataset of gridded land surface blend of Climatic Research Unit (CRU) and Japanese reanalysis (JRA) data.* Norwich: University of East Anglia.

Harris I.C. (2019b) A forcings dataset of gridded land surface blend of Climatic Research Unit (CRU) and Japanese reanalysis (JRA) data. CEDA Archive. Available at: https://doi.org/10.5285/13f3635174794bb98cf8ac4b0ee8f4ed. Accessed January 2020.

Hersbach H., Bell B., Berrisford P., Hirahara S., Horányi A., Muñoz-Sabater J., et al. (2020) The ERA5 global reanalysis. *Quarterly Journal of the Royal Meteorological Society*, 146(730), 1999–2049.

Hickler T., Smith B., Prentice I.C., Mjöfors K., Miller P., Arneth A., et al. (2008) CO2 fertilization in temperate FACE experiments not representative of boreal and tropical forests. *Global Change Biology*, 14(7), 1531–1542.

Hill T., Chocholek M. & Clement R. (2016) The case for increasing the statistical power of eddy covariance ecosystem studies: Why, where and how? *Global Change Biology*, 23, 2154–2165.

Hubau W., Lewis S.L., Phillips O.L., Affum-Baffoe K., Beeckman H., Cuní-Sanchez A., et al. (2020) Asynchronous carbon sink saturation in African and Amazonian tropical forests. *Nature*, 579(7797), 80-87.

Huntingford C. & Cox P.M. (2000) An analogue model to derive additional climate change scenarios from existing GCM simulations. *Climate Dynamics*, 16(8), 575–586.

Huntingford C., Harris P.P., Gedney N., Cox P.M., Betts R.A., Marengo J.A., et al. (2004) Using a GCM analogue model to investigate the potential for Amazonian forest dieback. *Theoretical and Applied Climatology*, 78(1-3), 177–185.

Huntingford C., Zelazowski P., Galbraith D., Mercado L.M., Sitch S., Fisher R.M.A., et al. (2013) Simulated resilience of tropical rainforests to CO2-induced climate change. *Nature Geoscience*, 6(4), 268–273.

Huntingford C., Jeffers E.S., Bonsall M.B., Christensen H.M., Lees T. & Yang H. (2019) Machine learning and artificial intelligence to aid climate change research and preparedness. *Environmental Research Letters*, 14, 124007.

IPCC. (2013) *Climate change 2013: The physical science basis. Contribution of Working Group I to the Fifth Assessment Report of the Intergovernmental Panel on Climate Change*. Cambridge, UK and New York, NY: Cambridge University Press.

Jackson R.B., Lajtha K., Crow S.E., Hugelius G., Kramer M.G. & Piñeiro G. (2017) The ecology of soil carbon: Pools, vulnerabilities, and biotic and abiotic controls. *Annual Review of Ecology, Evolution, and Systematics*, 48(1), 419–445.

Jardine K.J., Jardine A.B., Holm J.A., Lombardozzi D.L., Negron-Juarez R.I., Martin S.T., et al. (2017) Monoterpene "thermometer' of tropical forest-atmosphere response to climate warming. *Plant Cell and Environment*, 40(3), 441–452.

Jenkinson D.S. (1990) The turnover of organic-carbon and nitrogen in soil. *Philosophical Transactions of the Royal Society B-Biological Sciences*, 329(1255), 361–368.

Johnston A.S.A., Meade A., Ardö J., Arriga N., Black A., Blanken P.D., et al. (2021) Temperature thresholds of ecosystem respiration at a global scale. *Nature Ecology and Evolution*, 5, 487–494.

Jones C., Mcconnell C., Coleman K., Cox P., Falloon P., Jenkinson D., et al. (2005) Global climate change and soil carbon stocks; predictions from two contrasting models for the turnover of organic carbon in soil. *Global Change Biology*, 11(1), 154–166.

Jones C.D., Hughes J.K., Bellouin N., Hardiman S.C., Jones G.S., Knight J., et al. (2011) The HadGEM2-ES implementation of CMIP5 centennial simulations. *Geoscientific Model Development*, 4(3), 543–570.

Jones S., Rowland L., Cox P., Hemming D., Wiltshire A., Williams K., et al. (2020) The impact of a simple representation of non-structural carbohydrates on the simulated response of tropical forests to drought. *Biogeosciences*, 17(13), 3589–3612.

Jung M., Reichstein M., Ciais P., Seneviratne S.I., Sheffield J., Goulden M.L., et al. (2010) Recent decline in the global land evapotranspiration trend due to limited moisture supply. *Nature*, 467(7318), 951–954.

Jung M., Schwalm C., Migliavacca M., Walther S., Camps-Valls G., Koirala S., et al. (2020) Scaling carbon fluxes from eddy covariance sites to globe: Synthesis and evaluation of the FLUXCOM approach. *Biogeosciences*, 17(5), 1343–1365.

Kattge J. & Knorr W. (2007) Temperature acclimation in a biochemical model of photosynthesis: A reanalysis of data from 36 species. *Plant Cell and Environment*, 30(9), 1176–1190.

Keenan T.F., Migliavacca M., Papale D., Baldocchi D., Reichstein M., Torn M., et al. (2019) Widespread inhibition of daytime ecosystem respiration. *Nature Ecology and Evolution*, 3, 407–415.

Knohl A. & Baldocchi D.D. (2008) Effects of diffuse radiation on canopy gas exchange processes in a forest ecosystem. *Journal of Geophysical Research*, 113, G02023.

Kobayashi S., Ota Y., Harada Y., Ebita A., Moriya M., Onoda H., et al. (2015) The JRA-55 reanalysis: General specifications and basic characteristics. *Journal of the Meteorological Society of Japan*, 93(1), 5–48.

Körner C. (2015) Paradigm shift in plant growth control. *Current Opinion in Plant Biology*, 25, 107–114.

Lewis S.L., Lloyd J., Sitch S., Mitchard E.T.A. & Laurance W.F. (2009) Changing ecology of tropical forests: Evidence and drivers. *Annual Review of Ecology Evolution, and Systematics*, 40, 529–549.

Liu Y., Piao S., Gasser T., Ciais P., Yang H., Wang H., et al. (2019) Field-experiment constraints on the enhancement of the terrestrial carbon sink by CO2 fertilization. *Nature Geoscience*, 12(10), 809–814.

Lloyd J. & Taylor J.A. (1994) On the temperature-dependence of soil respiration. *Functional Ecology*, 8(3), 315–323.

Malavelle F.F., Haywood J.M., Mercado L.M., Folberth G.A., Bellouin N., Sitch S., et al. (2019) Studying the impact of biomass burning aerosol radiative and climate effects on the Amazon rainforest productivity with an Earth system model. *Atmospheric Chemistry and Physics*, 19(2), 1301–1326.

Malhi Y., Aragao L.E.O.C., Galbraith D., Huntingford C., Fisher R., Zelazowski P., et al. (2009) Exploring the likelihood and mechanism of a climate-change-induced dieback of the Amazon rainforest. *Proceedings of the National Academy of Sciences of the United States of America*, 106(49), 20610–20615.

Meinshausen M., Smith S.J., Calvin K., Daniel J.S., Kainuma M.L.T., Lamarque J.F., et al. (2011) The RCP greenhouse gas concentrations and their extensions from 1765 to 2300. *Climatic Change*, 109(1-2), 213–241.

Mercado L.M., Bellouin N., Sitch S., Boucher O., Huntingford C., Wild M., et al. (2009) Impact of changes in diffuse radiation on the global land carbon sink. *Nature*, 458(7241), 1014-U87.

Mercado L.M., Medlyn B.E., Huntingford C., Oliver R.J., Clark D.B., Sitch S., et al. (2018) Large sensitivity in land carbon storage due to geographical and temporal variation in the thermal response of photosynthetic capacity. *New Phytologist*, 218(4), 1462–1477.

Moore J.R., Argles A.P.K., Zhu K., Huntingford C. & Cox P.M. (2020) Validation of demographic equilibrium theory against tree-size distributions and biomass density in Amazonia. *Biogeosciences*, 17(4), 1013–1032.

Moore J.R., Zhu K., Huntingford C. & Cox P.M. (2018) Equilibrium forest demography explains the distribution of tree sizes across North America. *Environmental Research Letters*, 13, 084019.

Nottingham A.T., Meir P., Velasquez E. & Turner B.L. (2020) Soil carbon loss by experimental warming in a tropical forest. *Nature*, 584(7820), 234–237.

Palmer T. & Stevens B. (2019) The scientific challenge of understanding and estimating climate change. *Proceedings of the National Academy of Sciences of the United States of America*, 116(49), 24390–24395.

Phillips O.L., Lewis S.L., Higuchi N. & Baker T. (2016) Recent changes in Amazon forest biomass and dynamics. In: L. Nagy, B.R. Forsberg and P. Artaxo (Editors), *Interactions between biosphere, atmosphere and human land use in the Amazon basin*. Berlin: Springer, pp. 191–224.

Quesada C.A., Phillips O.L., Schwarz M., Czimczik C.I., Baker T.R., Patiño S., et al. (2012) Basin-wide variations in Amazon forest structure and function are mediated by both soils and climate. *Biogeosciences*, 9(6), 2203–2246.

Ryu Y., Jiang C., Kobayashi H. & Detto M. (2018) MODIS-derived global land products of shortwave radiation and diffuse and total photosynthetically active radiation at 5 km resolution from 2000. *Remote Sensing of Environment*, 204, 812–825.

Sellar A.A., Jones C.G., Mulcahy J.P., Tang Y., Yool A., Wiltshire A., et al. (2019) UKESM1: Description and evaluation of the UK Earth System Model. *Journal of Advances in Modeling Earth Systems*, 11(12), 4513–4558.

Sitch S., Huntingford C., Gedney N., Levy P.E., Lomas M., Piao S.L., et al. (2008) Evaluation of the terrestrial carbon cycle, future plant geography and climate-carbon cycle feedbacks using five Dynamic Global Vegetation Models (DGVMs). *Global Change Biology*, 14, 2015–2039.

Sitch S., Friedlingstein P., Gruber N., Jones S.D., Murray-Tortarolo G., Ahlström A., et al. (2015) Recent trends and drivers of regional sources and sinks of carbon dioxide. *Biogeosciences*, 12, 653–679.

Sullivan M.J.P., Lewis S.L., Affum-Baffoe K., Castilho C., Costa F., Sanchez A.C., et al. (2020) Long-term thermal sensitivity of Earth's tropical forests. *Science*, 368(6493), 869-874.

Sun Y., Goll D.S., Chang J., Ciais P., Guenet B., Helfenstein J., et al. (2021) Global evaluation of the nutrient-enabled version of the land surface model ORCHIDEE-CNP v1.2 (r5986). *Geoscientific Model Development*, 14, 1987–2010.

Taylor K.E., Stouffer R.J. & Meehl G.A. (2012) An overview of CMIP5 and the experiment design. *Bulletin of the American Meteorological Society*, 93(4), 485–498.

Terrer C., Jackson R.B., Prentice I.C., Keenan T.F., Kaiser C., Vicca S., et al. (2019) Nitrogen and phosphorus constrain the CO_2 fertilization of global plant biomass. *Nature Climate Change*, 9(9), 684–689.

Vitousek P.M. (1984) Litterfall, nutrient cycling, and nutrient limitation in tropical forests. *Ecology*, 65(1), 285–298.

Wang Y., Sperry J.S., Anderegg W.R.L., Venturas M.D. & Trugman A.T. (2020) A theoretical and empirical assessment of stomatal optimization modeling. *New Phytologist*, 227(2), 311–325.

Wang Y.-P. & Goll D.S. (2021) Modelling of land nutrient cycles: Recent progress and future development. *Faculty Reviews*, 10, 53.

Wiltshire A.J., Burke E.J., Chadburn S.E., Jones C.D., Cox P.M., Davies-Barnard T., et al. (2021) JULES-CN: A coupled terrestrial carbon-nitrogen scheme (JULES vn5.1). *Geoscientific Model Development*, 14, 2161–2186.

Yang X., Thornton P.E., Ricciuto D.M. & Hoffman F.M. (2016) Phosphorus feedbacks constraining tropical ecosystem responses to changes in atmospheric CO_2 and climate. *Geophysical Research Letters*, 43, 7205–7214.

Yuan H., Dai Y., Dickinson R.E., Pinty B., Shangguan W., Zhang S., et al. (2017) Reexamination and further development of two-stream canopy radiative transfer models for global land modeling. *Journal of Advances in Modeling Earth Systems*, 9, 113–129.

SUPPORTING INFORMATION

Additional supporting information may be found in the online version of the article at the publisher's website.

How to cite this article: Huntingford C., Sitch S.A. & O'Sullivan M. (2022) Impact of merging of historical and future climate data sets on land carbon cycle projections for South America. *Climate Resil Sustain*, 1, e24. https://doi.org/10.1002/cli2.24